# Albumin-based nanoparticles as methylprednisolone carriers for targeted delivery towards the neonatal Fc receptor in glomerular podocytes

LIN WU*, MINGYU CHEN*, HUIJUAN MAO, NINGNING WANG, BO ZHANG, XIUFEN ZHAO, JUN QIAN and CHANGYING XING

Department of Nephrology, The First Affiliated Hospital of Nanjing Medical University, Nanjing, Jiangsu 210029, P.R. China

Received April 11, 2016; Accepted February 16, 2017

DOI: 10.3892/ijmm.2017.2902

**Abstract.** Glucocorticoids (GCs) are commonly used in the treatment of nephrotic syndrome. However, high doses and long periods of GC therapy can result in severe side effects. The present study aimed to selectively deliver albumin-methylprednisolone (MP) nanoparticles towards glomerular podocytes, which highly express the specific neonatal Fc receptor (FcRn) of albumin. Bovine serum albumin (BSA) was labeled with a fluorescent dye and linked with modified MP via an amide bond. The outcome nanoparticle named BSA633-MP showed a uniform size with a diameter of approximately 10 nm and contained 12 drug molecules on average. The nanoconjugates were found to be stable at pH 7.4 and acid-sensitive at pH 4.0, with approximately 72% release of the MP drug after 48 h of incubation. The nanoparticle demonstrated a 36-fold uptake in receptor-specific cellular delivery in the FcRn-expressing human podocytes compared to the uptake in the non-FcRn-expressing control cells. Co-localization further confirmed that uptake of the nanoconjugates involved receptor-mediated endocytosis followed by lysosome associated transportation. *In vitro* cellular experiments indicated that the BSA633-MP ameliorated puromycin aminonucleoside-induced podocyte apoptosis. Moreover, *in vivo* fluorescence molecular imaging showed that BSA633-MP was mainly accumulated in the liver and kidney after intravenous dosing for 24 h. Collectively, this study may provide an approach for the effective and safe therapy of nephrotic syndrome.

*Correspondence to:* Professor Changying Xing, Department of Nephrology, The First Affiliated Hospital of Nanjing Medical University, 300 Guangzhou Road, Nanjing, Jiangsu 210029, P.R. China
E-mail: cyxing62@126.com

*Contributed equally

*Key words:* albumin, glucocorticoids, nanoparticles, nephrotic syndrome, podocytes

## Introduction

Nephrotic syndrome is basically characterized by massive proteinuria. Reducing urinary protein is not only one of the key goals in the treatment of nephrotic syndrome, but also the decisive factor in improving the prognosis. To date, glucocorticoid (GC) therapy still remains the first-line treatment for proteinuria glomerular nephropathy and is widely used in nephrotic syndrome including membranous nephropathy (MN), minimal-change disease (MCD), focal segmental glomerulosclerosis (FSGS), and lupus nephritis (LN), which are all characterized by podocyte injury and proteinuria (1-3).

It is well-known that podocytes play an important role in maintaining normal glomerular structure and function. Increasing number of studies has shown that podocyte damage or loss is the key factor which affects the glomerular filtration barrier and causes proteinuria (4,5). Present studies indicate that GCs can directly act on podocytes. It has been demonstrated that there are functional receptors for GCs on glomerular podocytes (6). Many *in vitro* experiments have demonstrated that GCs could protect or promote repair of podocytes from injury (7-13). Although GC therapy has shown prominent efficacy in nephrotic syndrome and thereby improves the survival of patients, unfortunately, the serious side effects of GCs such as bone mobilization, muscle mass loss, immunosuppression, and metabolic alterations have limited their clinical application. Thus, it is clear that alternative therapies with greater efficacy and/or fewer side effects are crucially needed.

Nanoparticle-based delivery has become an important strategy by which to target GCs to specific locations. To achieve targeted delivery, a ligand on the delivery system binds to its receptor on the surface of diseased cells and then undergoes receptor-mediated endocytosis, so as to overcome wide systemic side effects when GCs are administered in the free form. Many approaches have been undertaken to obtain such a goal in different fields. For example, milatuzumab, a humanized monoclonal antibody directed against CD74, was conjugated to liposomes as a targeted dexamethasone carrier for therapeutic delivery in $CD74^+$ B-cell malignancies (14). An anti-CD163 antibody-dexamethasone conjugate was developed in order to specifically target GC to the hemoglobin scavenger receptor CD163 in macrophages (15). Targeted GCs have also

been used in renal diseases. Dexamethasone was encapsulated in liposome modified with monoclonal antibodies against E-selectin, which is specifically expressed on activated glomerular endothelium in glomerulonephritis (16,17).

There is a close link between podocyte injury and proteinurea. However, research concerning the targeted delivery toward podocytes has not been reported. The key goal is to identify a specific receptor expressed on podocytes. The so-called neonatal Fc receptor (FcRn) is a cell surface glycoprotein which is a major IgG Fc receptor capable of facilitating the translocation of IgG. Recent evidence suggests that FcRn is a key and promising target in IgG-related drug delivery and disease therapy (18). Besides acting as the receptor of IgG, FcRn is also a natural receptor of albumin. Eyre *et al* found that mouse and human podocytes are able to specifically endocytose albumin (19). Haymann demonstrated the presence of FcRn on glomerular podocytes as well as in the brush border of proximal tubular cells (20). In the present study, it was found that FcRn is abundantly expressed in human podocytes in renal biopsy specimens with nephritic syndrome, including MCD, FSGS, MN, LN and diabetic nephropathy (DN).

It is well-known that the trapped molecular size of the normal glomerular filtration barrier is approximately 7 nm, which happens to be the same as the diameter of the albumin molecule. Under normal circumstances, only little albumin can be transported across the glomerular filtration barrier. However, when nephritic syndrome occurs, the glomerular permeability is significantly increased and a large amount of albumin passes through the basement membrane to reach the podocyte side. Based on the above understanding, we designed a nanoparticle consisted of albumin and GC molecules. Such a delivery system may have dual-targeting effects. Firstly, the albumin-carrying drug can pass through the diseased glomerular filtration barrier. Secondly, albumin can be recognized by FcRn expressed on podocytes, where GC molecules can be released and exert their active effect.

## Materials and methods

*Localization of FcRn in human glomeruli.* Immunofluorescence was performed to study the presence of FcRn using renal biopsy specimens with nephrotic syndrome in different pathological types including MCD, FSGS, MN, LN, mesangial proliferative glomerulonephritis (MsPGN) and DN. The present study was approved by the Ethics Committee of The First Affiliated Hospital of Nanjing Medical University (Nanjing, China). The rabbit anti-FcRn polyclonal antibody (Cat. no. HPA012122) was purchased from Sigma-Aldrich (St. Louis, MO, USA). Briefly, 3 $\mu$m-thick cryostat sections were fixed in 4% paraformaldehyde for 10 min and washed in PBS. The sections were incubated with anti-FcRn antibody at a dilution of 1:400 overnight at 4˚C, washed with PBS, and incubated with FITC-labeled anti-rabbit IgG (Cat. no. ZF-0311; ZSGB-Bio, Beijing, China) for 3 h at 37˚C. A rabbit isotype IgG was used as the negative control to confirm FcRn specificity. Double staining was performed using a mouse monoclonal antibody to synaptopodin (Cat. no. 03-61094) at a dilution of 1:30 (American Research Products Inc., Waltham, MA, USA) a podocyte marker, and a Texas red-labeled anti-mouse IgG (Cat. no. ZF-0513; ZSGB-Bio) for detection. The fluorescence intensity level was judged by a renal pathologist under single-blind situation. Images were captured using fluorescence microscopy.

*Synthesis of albumin-based nanoconjugates.* The overall strategy was to covalently conjugate the GC methylprednisolone (MP) to the albumin carrier which is the ligand of FcRn. Firstly, bovine serum albumin (BSA; Sigma-aldrich) was labeled with a fluorescent dye at Cys-34 by reacting it with Alexa Fluor 633 C5 Maleimide (Gibco Life Technologies, Carlsbad, CA, USA) at a 1:2 molar ratio of protein to dye in PBS supplemented with 1 mM EDTA (pH 7.0) for 2 h at room temperature. The labeled BSA was purified by gel filtration using a G-25 Desalting Column (GE Healthcare, Piscataway, NJ, USA). The protein concentration of BSA633 was measured by BCA assay. Secondly, the drug that will be conjugated to BSA was activated. Briefly, MP-hemisuccinate 9.5 mg, 20 $\mu$mol (Wuhan E-ternity Technologies Co., Ltd, China) was dissolved in 100 $\mu$l anhydrous DMSO to form a 200 mM concentrated solution. An amount of 2 mg Sulfo-N-hydroxysuccinimide (Sulfo-NHS; Thermo Fisher Scientific, Waltham, MA, USA) was dissolved in 50 $\mu$l $H_2O$ and 2 mg N-ethyl-N'-(3-dimethylaminopropyl) carbodiimide (EDC; Thermo Fisher Scientific) in 40 $\mu$l $H_2O$ to form a solution of 200 mM (EDC) and 230 mM (Sulfo-NHS), respectively. An amount 1 $\mu$l of 200 mM MP-hemisuccinate solution was added to 1 ml MES solution (0.1M MES, 0.5 M NaCl, pH 6.0), and 10 $\mu$l of 200 mM EDC solution was added to give ~10 moles of EDC for each mole of drug. An amount 22 $\mu$l of 230 mM Sulfo-NHS solution was added to the above solution. The reaction was allowed to proceed for 15 min at room temperature. EDC was quenched by 1.4 $\mu$l of 2-mercaptoethanol (final concentration of 20 mM). The pH was increased to 7.2 with concentrated phosphate buffer immediately before reaction to protein. Lastly, purified BSA633 was added to the activated drug solution at a molar ratio of 1:30. The mixture was allowed to remain at room temperature for 2 h. The final product was subsequently diafiltered using spin filters (Amicon-Ultra, 30K; EMD Millipore, Billerica, MA, USA) into PBS pH 7.4 to remove the excess raw materials and other byproducts. Samples were stored at 4˚C for future analysis.

*Characterization of BSA633-MP.* In order to observe the integrity and polymerization of the final products, a non-reduced SDS-PAGE was carried out using 12% polyacrylamide gel without 2-mercaptoethanol. After electrophoresis, the gel was stained with Coomassie Blue R-250 and destained in 45:10:45 (methanol:glacial acetic acid:water).

The size of the nanoconjugates and BSA was also confirmed with transmission electron microscopy (TEM). In this experiment, the nanoconjugates were diluted to 0.05 mg/ml and dropped on 200 mesh carbon-coated copper grids (Ted Pella Inc., Redding CA, USA) and allowed to attach for 2 min. A concentration of 2% phosphotungstic acid was used to counterstain the nanoparticles. Samples were viewed using a TECNAI G2 F30 transmission electron microscope (FEI, Eindhoven, The Netherlands).

The number of MP linked to BSA was further determined by matrix-assisted laser desorption ionization (MALDI)

mass spectrometry with time-of-fight (TOF) using 5800 MALDI-TOF-TOF MS-MS instrument (AB SCIEX, Foster City, CA, USA). An aliquot (1 $\mu$l) of the sample solution was mixed with an equal aliquot of the matrix solution [2,5-dihydroxybenzoic acid (DHB) in 30% acetonitrile and 0.1% trifluoroacetic acid] and 1 $\mu$l of the mixed solution was spotted onto the target plate and evaporated under a gentle stream of warm air. Mass spectra were acquired in positive reflector mode. The accelerating voltage was 25 kV.

The purity of BSA633-MP was determined at 254 nm with an analytical HPLC-Gel-Filtration column (TSKgel G3000PWXL, 300x7.8 mm; TOSOH Corporation, Tokyo, Japan) according to the manufacturer's instructions (mobile phase: 0.15 M NaCl, 0.01 M $NaH_2PO_4$, 5% $CH_3CN$, pH 7.0).

*PH-dependent stability of BSA633-MP.* The amide bond between MP and BSA was sensitive to strong acid and alkali. Our previous study confirmed this conclusion in which the conjugates formed in the amide bond underwent hydrolysis over 60% under pH 4.0 for 48 h (21). In this study, conjugates were incubated in PBS at pH 7.4 and acetate buffer at pH 4.0 for 48 h at 37˚C. A time course release assay (1, 4, 8, 12, 24 and 48 h) was also carried out at pH 4 and 37˚C. After incubation, samples were eluted in a column with Sephadex G-100 gel (Sigma-Aldrich). The MP contents in the fractions were then detected by OD240 (with subtraction of albumin itself), while the albumin was detected by Alexa Fluor 633.

*Cell culture.* Conditionally immortalized human podocytes were kindly provided by Dr Moin A. Saleem (University of Bristol, Southmead Hospital, Bristol, UK). The human podocytes were cultured in RPMI-1640 medium (Life Technologies, Grand Island, NY, USA, USA) supplemented with 10% FBS (Gibco, Grand Island, NY, USA) at a permissive temperature (33˚C). When the podocytes reached ~70-80% confluence at 33˚C, the podocytes were transferred at 37˚C for differentiation. Renal tubular cell line HK-2, with high expression of FcRn, was maintained in F12 medium containing 10% FBS. Vascular smooth muscle cells (VSMCs), which lack FcRn expression, were used as the negative control. VSMCs were cultured in Dulbecco's modified Eagle's medium (DMEM) supplemented with 10% FBS.

*Quantitative polymerase chain reaction (qPCR).* Total RNA was isolated from human podocytes as well as HK-2 cells and VSMCs with Trizol (Invitrogen Life Technologies, Carlsbad, CA, USA) according to the manual. cDNA was synthesized from 1 $\mu$g of total RNA using a reverse transcription kit (Thermo Fisher Scientific). 18S rRNA served as an internal control. Primer sequences were as follows: FcRn forward, 5'-CTGAGAACGGAAATCGTTGCTAA-3' and reverse, 5'-TTAGCAGGAACTCGCTCTCCTT-3'; 18S forward, 5'-CATGATTAAGAGGGACGGC-3' and reverse, 5'-TTC AGCTTTGCAACCATACTC-3'. qPCR was performed in duplicate with 0.2 $\mu$M primers, 1 $\mu$l cDNA and SYBR-Green Real-Time PCR Master Mix (Roche Applied Science, Mannheim, Germany) in a total volume of 20 $\mu$l. Reactions were run at 95˚C for 60 sec, followed by 40 cycles of 15 sec at 95˚C, 15 sec at 60˚C and 45 sec at 72˚C. The StepOnePlus™ Real-Time PCR system (Applied Biosystems Life Technologies, Foster City, CA, USA) was used for analysis. Results are expressed as cycle threshold (Ct) and calculated as ΔCt, which were normalized to endogenous control 18S rRNA.

*Cellular uptake.* Total cellular uptake of the Alexa Fluor 633-labeled nanoconjugate was measured by flow cytometry using a BD FACSCalibur flow cytometer (Becton-Dickinson, San Jose, CA, USA) and data were analyzed using CellQuest software (Becton-Dickinson). Before treatment, cell medium was changed and cells were washed 3 times with PBS, and then the conjugate in serum-free Opti-MEM was added to the wells. After treatment with the labeled BSA633-MP for 6 h, the cells were trypsinized and were analyzed by flow cytometry, with a 639 nm laser coupled with a 675-20 emission filter for Alexa Fluor 633.

*Confocal fluorescence microscopy.* Confocal microscopy was performed to examine the subcellular distribution of the targeted nanoconjugates. The differentiated human podocytes were incubated with BSA633-MP in Opti-MEM® media for 4 h. Thereafter, the cells were washed with PBS and treated with Lysotracker Green DND-26 (75 nM) which was used to track lysosomes for 2 h. Cells were imaged with confocal microscope (Olympus FV1000; Olympus Corp., Tokyo, Japan) using 488 and 633 nm laser and merged to determine the intracellular localization of the BSA633-MP nanoconjugates.

*Cell viability assay.* The cytoprotective ability of the nanoconjugates was measured with the CCK-8 assay (Dojindo Molecular Technologies, Inc., Kumamoto, Japan). In brief, human podocytes were seeded in 96-well plates at 3,000 cells/well in a 100 $\mu$l volume overnight. Then medium was replaced and exposed to different concentrations of puromycin aminonucleoside (PAN) for 48 h. After a suitable dose was determined, dosing for different periods (12, 24 or 48 h) was performed. Then PAN at optimal concentration and period was administered to podocytes with or without the free MP or BSA633-MP nanoconjugates. CCK-8 solution (10 $\mu$l) was added and incubated at 37˚C for 4 h. The optical density (OD) of the plates was read at 450 nm using a plate reader.

*In vivo and ex vivo imaging.* Female BALB/c mice were purchased from Shanghai SLAC Laboratory Animal Co., Ltd., Shanghai, China. Mice were maintained under a 12-h light-dark cycle and had access to food and water *ad libitum*. All experiments were approved by the Institutional Animal Care and Use Committee of Nanjing Medical University.

The near infrared dye Alexa Fluor 633 was conjugated to the BSA carrier to monitor the biodistribution and targeting efficacy of the nanoconjugates. The mice were intravenously injected with 200 $\mu$l of BSA633-MP nanoconjugates in PBS at 10 $\mu$M in terms of BSA (n=3). After 24 h, the mice were anesthetized with 2% isoflurane. Whole body optical imaging was carried out using a small-animal optical molecular imaging system (VIS Imaging Spectrum System; Caliper Life Sciences, Hopkinton, MA, USA) equipped with fluorescent filter sets (excitation-emission, 633/647 nm). Fluorescence images were normalized and reported as counts per second (count/sec). In order to observe more concisely, mice were then sacrificed and

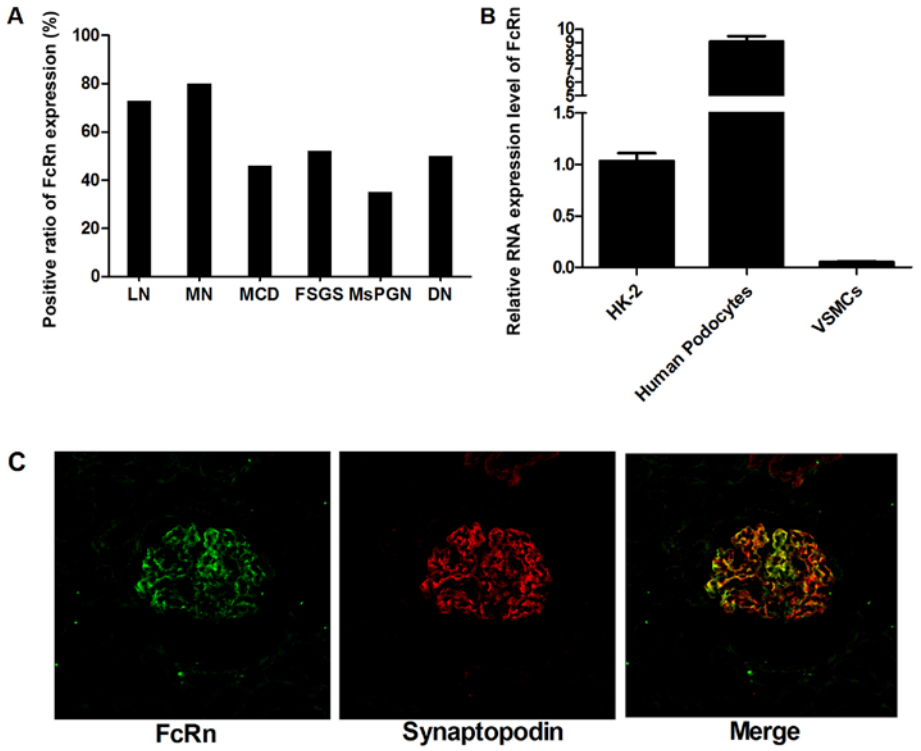


Figure 1. Localization of the neonatal Fc receptor (FcRn) in human glomeruli and mRNA expression level of FcRn in human podocytes. (A) Immunofluorescence was performed to study the presence of FcRn in different pathological types of nephrotic syndrome including minimal-change disease (MCD), focal segmental glomerulosclerosis (FSGS), membranous nephropathy (MN), lupus nephritis (LN), mesangial proliferative glomerulonephritis (MsPGN) and diabetic nephropathy (DN). (B) Relative mRNA expression level of FcRn was assessed in human podocytes, HK-2 cells and vascular smooth muscle cells (VSMCs) using qPCR. (C) Double staining was performed using a mouse monoclonal antibody to synaptopodin, which is a marker of podocytes. Green image, GFP fluorescence representing FcRn detection. Red image, Texas red fluorescence representing synaptopodin expression.

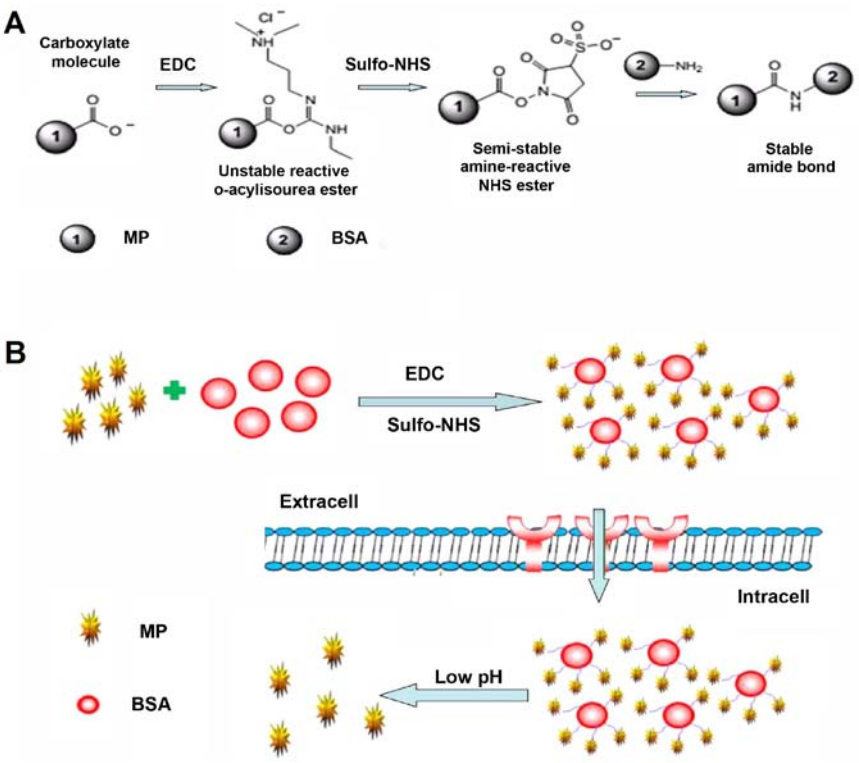


Figure 2. Preparation and targeted delivery of the BSA633-MP nanoconjugates. (A) The modified carboxyl of methylprednisolone (MP) was activated with Sulfo-N-hydroxysuccinimide (Sulfo-NHS) that formed an active ester group in the presence of N-ethyl-N'-(3-dimethylaminopropyl) carbodiimide (EDC). Then the free amino on the bovine serum albumin (BSA) carrier was crosslinked with the modified methylprednisolone to form BSA633-MP. (B) BSA633-MP was delivered into podocytes by endocytosis mediated by the BSA receptor, which was the so-called neonatal Fc receptor which is overexpressed on injured podocytes. MP was released to the cytoplasm from the conjugate under decreased pH condition.

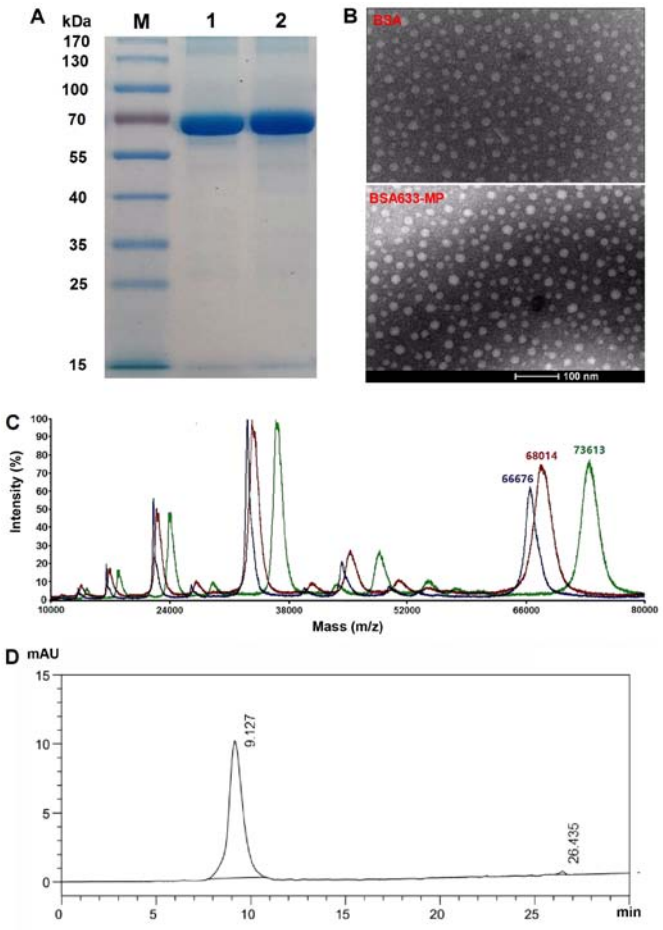


Figure 3. Size characterization of the BSA633-MP nanoconjugate. (A) SDS-PAGE gel electrophoresis of BSA633-MP. Lanes 1 and 2 indicate bovine serum albumin (BSA) carrier and BSA633-MP nanoconjugate, respectively. (B) Transmission electron microscopy image of BSA and BSA633-MP nanoconjugate. The sample was counterstained with 2% phosphotungstic acid. The average particle size was both estimated to be 10 nm. (C) MALDI-TOF MS of BSA (blue), BSA633 (red) and BSA633-MP (green). The increase in the molecular weight from 66,676 to 68,014 was due to Alexa Fluor 633 modification on BSA, while the increase from 68,014 to 73,613 was due to methylprednisolone modification. (D) Size-exclusion HPLC chromatogram of BSA633-MP conjugate showed that BSA633-MP had a high purification. Methylprednisolone (MP) molecules were mainly covalently bonded to BSA. Peak eluted at 9.1 and 26.4 min referred to BSA-633-MP conjugate and free MP, respectively.

organs including the heart, liver, spleen, lung and kidney were obtained for fluorescence imaging.

*Data analysis*. Data are presented as mean ± standard error of the mean from at least three experiments. Statistical significance was evaluated using the Student's t-test. $P<0.05$ was considered to indicate a statistically significant difference.

## Results

*FcRn expression in human glomeruli and cultured human podocytes*. A total of 105 renal biopsy specimens with nephrotic syndrome of different pathological types including MCD, FSGS, MN, MsPGN, LN and DN were subjected to immunofluorescence to identify the expression of FcRn. The detailed positive ratio is presented in Fig. 1A. It was observed that FcRn was expressed in all the pathological types. Among these, MN and LN samples showed a relatively higher positive rate for FcRn staining. Fig 1C shows double staining which was performed using the synaptopodin and FcRn antibodies simultaneously, in which FcRn and synaptopodin expression had obvious coincident sites. As synaptopodin is a molecular marker of podocytes, we regarded that the expression of FcRn in human glomeruli was attributed to the podocytes. Notably, a negative result was obtained when a rabbit isotype IgG was used as a negative control antibody instead of the anti-FcRn antibody, which confirmed the specificity of the anti-FcRn antibody. As the negative result was almost black, it was not presented here. Then the RNA level of FcRn expressed in human podocytes was assayed by RT-PCR analysis. The HK-2 cell line was used as positive control and VSMCs as a negative control. As shown in Fig 1B, the RNA level of FcRn expression was ~8-fold higher in the human podocytes than it was in the HK-2 cells and was ~400-fold higher than the level in the negative VSMC control. This was consistent with the previous immunofluorescent results, confirming FcRn as a suitable target for albumin-mediated drug delivery.

*Synthesis and characterization of the BSA633-MP nanoconjugates*. The overall strategy for preparation of the nanoconjugates is outlined in Fig. 2. First, the single sulfhydryl group on BSA was labeled with the far red fluorophore Alexa Fluor 633. Subsequently, MP-hemisuccinate was reacted to Sulfo-NHS in the presence of EDC. The activated Sulfo-NHS ester was then reacted with the surface amino groups of BSA to form amide crosslink. The targeted nanoconjugates were then termed BSA633-MP.

*The molecular size of the nanoconjugates was estimated using non-reducing SDS-PAGE and TEM*. The integrity of the synthesized BSA633-MP conjugates was evaluated by SDS-PAGE. The single band corresponding to BSA633-MP is shown in Fig. 3A, suggesting that the conjugate was mostly synthesized as a monomer. Furthermore, the band representing BSA633-MP was almost at the same position as BSA itself, without visible molecular mass increase. The molecular size of the BSA633-MP conjugates was further confirmed by TEM, which revealed an average diameter of 10 nm, consistent with the SDS-PAGE result (Fig. 3B). The number of MP linked to BSA was further determined by MALDI-TOF mass spectrometry. As shown in Fig 3C, a typical increase (~5,600 kDa) in the molecular weight of BSA633-MP compared with BSA633 implied that the amount of drug conjugated was ~12 molecules per albumin (Mw = 474.54), showing high payloads. To note, other peaks represented molecules with different charges. For example, peaks of BSA of ~33,000 and 22,000 kDa indicated that the number of charge was 2 and 3, respectively.

In order to discern between associated MP (adhered to BSA) and truly conjugated MP, Gel-Filtration HPLC was applied. The absorption wavelength of 254 nm was chosen for detection of MP (Fig. 3D). The main peak at 9.1 min corresponded to the BSA633-MP conjugate, while MP was eluted at 26.4 min. The final product contained <2% MP, suggesting the successful conjugation of MP to BSA as well as high purity of the conjugate.

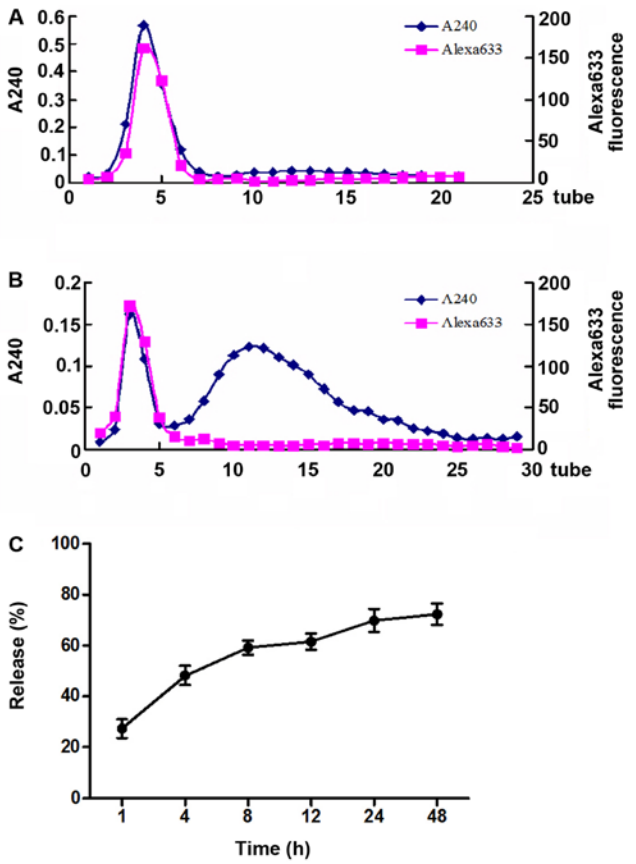


Figure 4. Effect of pH on the release of methylprednisolone (MP) from the BSA633-MP nanoconjugate. The nanoconjugates were incubated in (A) PBS at pH 7.4 and (B) acetate buffer at pH 4.0 for 48 h at 37˚C. After incubation, samples were eluted in a column with Sephadex G-100 gel. An amount of 0.5 ml of each fraction was collected. The released MP was detected by OD240, while albumin was detected by Alexa Fluor 633. (C) The nanoconjugates were incubated at pH 4.0 for 1, 4, 8, 12, 24 and 48 h at 37˚C for a time course release assay. Values are the mean ± standard error of the mean (n=3).

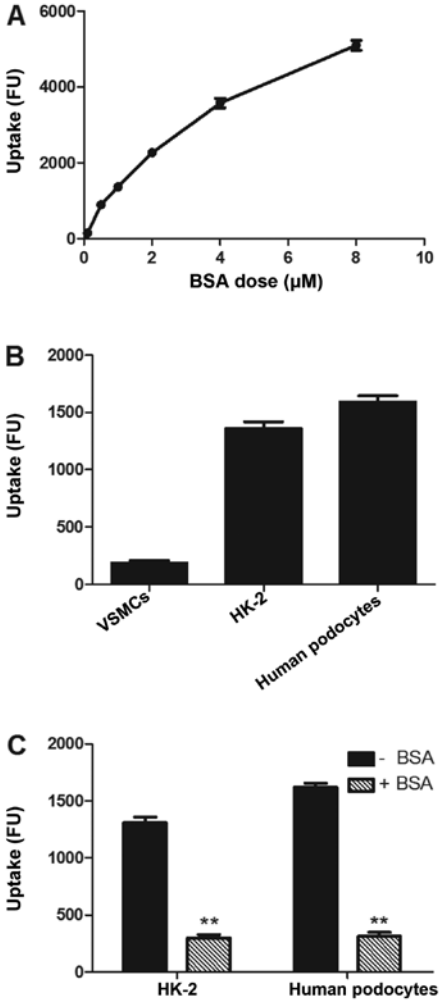


Figure 5. Cellular uptake of the BSA633-MP nanoconjugate. (A) Human podocytes were treated with increasing concentrations of BSA633-MP (equal to 0.1-8 $\mu$M BSA) for 6 h followed by flow cytometric measurement. (B) Uptake of BSA633-MP (BSA 1 $\mu$M) was compared in human podocytes, HK-2 cells and VSMCs. After 6 h of incubation, total cellular uptake of Alexa Fluor 633-labeled nanoconjugate was measured by flow cytometry. (C) Human podocytes were treated with BSA633-MP containing 1 $\mu$M bovine serum albumin (BSA) in the absence and presence of excess free BSA (1.5 mM) for 6 h and then total cellular uptake was measured. Data represent mean ± standard error of the mean of a representative experiment in triplicate. $^{**}$P<0.001.

*Release profile of BSA633-MP*. The effects of neutral pH and relatively acidic pH on the release profile of BSA633-MP conjugate were evaluated. As shown in Fig. 4A, we clearly see that under pH 7.4, almost nothing was released from the BSA633-MP conjugate. However, under pH 4.0, most MP molecules were released, a small unreleased portion remained which was eluted together with albumin (Fig. 4B). The OD240 values involved in the second elution peak vs. the total OD240 values (with subtraction of albumin itself) were calculated to roughly estimate the release percentage. As shown in Fig. 4C, with prolonged incubation, drug release was increased and at 48 h the release almost reached a plateau. Under pH 4.0 ~72% of MP drug was released after 48 h. These results indicated that the BSA633-MP conjugate was acid-sensitive and very stable in a neutral environment. Actually, the nanoconjugates were found to be stable for at least 3 months when stored in buffer at pH 7.4, without manifesting aggregation or degradation (data not shown).

*Cellular uptake of BSA633-MP conjugates*. The cellular uptake of the BSA633-MP nanoconjugates was evaluated by incubating cells with the conjugates for 6 h and then measuring total cell-associated fluorescence by flow cytometry. As shown in Fig. 5A, the uptake of the nanoconjugates was dose-dependent based on BSA concentration. The uptake of the nanoconjugates was well described by a classic saturable michaelismenten model, which is consistent with a saturable, receptor-mediated endocytosis. Uptake of the targeted nanoconjugates was contrasted in FcRn-positive and -negative cells. As shown in Fig. 5B, the uptake of nanoconjugates was 36- and 29-fold higher in the human podocytes and HK-2-positive control cells than that in the VSMCs which lack the FcRn receptor. Moreover, co-incubation with excess amounts of free BSA (1.5 mM) led to obvious inhibition of uptake of the nanoconjugates (Fig. 5C). These observations support the concept that the cellular uptake of the BSA conjugates depends on FcRn receptor-mediated endocytosis.

*Intracellular trafficking of BSA633-MP conjugates*. Through confocal microscopy, we observed the subcellular distribution of BSA633-MP conjugates. As shown in Fig. 6A, human podocytes treated with BSA633-MP conjugates for 4 h displayed

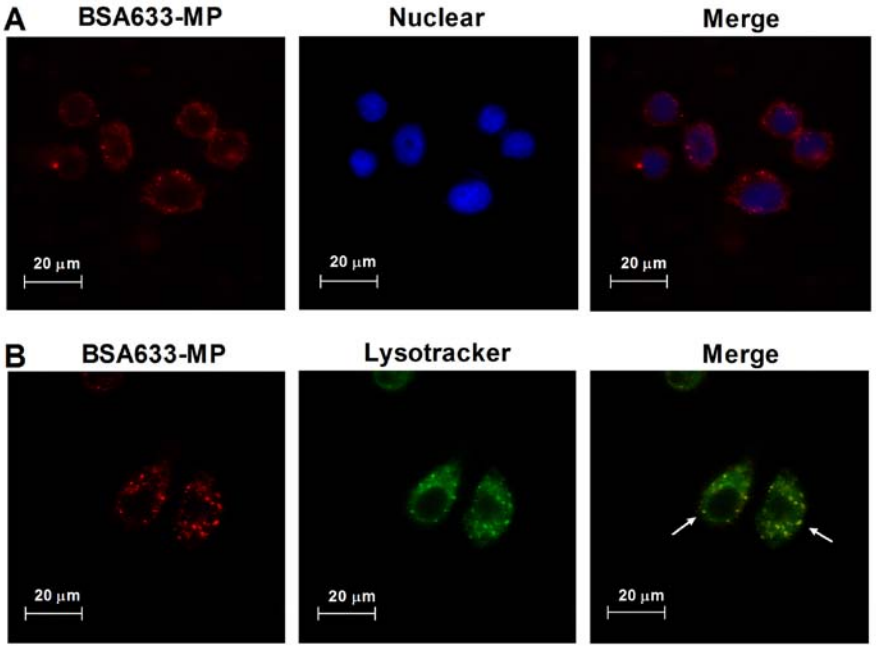


Figure 6. Subcellular localization of the BSA633-MP nanoconjugate. Human podocytes were incubated with Alexa Fluor 633-labeled BSA633-MP nanoconjugate containing 1 $\mu$M bovine serum albumin (BSA) for 4 h, and (A) cell nuclei were stained with DAPI. (B) Cells were treated with Lysotracker for 2 h which was used to track lysosomes. Cells were then observed by confocal microscopy. Green image, GFP fluorescence; red image, Alexa Fluor 633 fluorescence; blue image, DAPI fluorescence. The obtained results indicate that the nanoconjugate was localized in the lysosome.

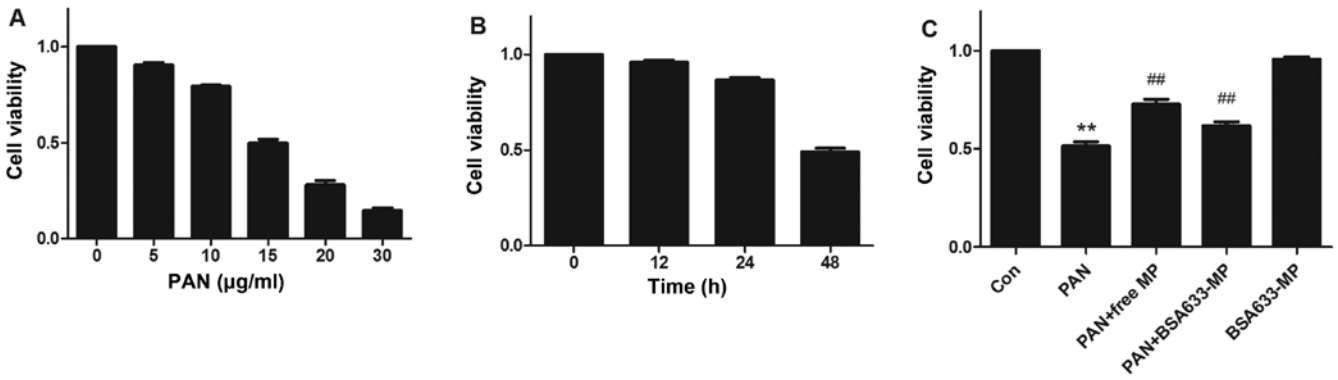


Figure 7. Cytoprotective ability of the BSA633-MP nanoconjugates. (A) Different doses of puromycin aminonucleoside (PAN) were administered to human podocytes for 48 h. (B) Human podocytes were treated with 15 $\mu$g/ml of PAN for different time periods. (C) Human podocytes were treated with 15 $\mu$g/ml of PAN in the absence or presence of 1 $\mu$M of free methylprednisolone (MP) or BSA633-MP nanoconjugates (equal to 1 $\mu$M MP) for 48 h. The cytoprotective ability of the nanoconjugates was measured with the CCK-8 assay. Cell viability of control cells was set as 100%. The nanoconjugates protected human podocytes from being injured by PAN as well as free MP. Data represent mean ± standard error of the mean in triplicate experiments. $^{**}$P<0.001 vs. the control group; $^{\#\#}$P<0.001 vs. the PAN group.

intracellular red fluorescence. Lysotracker was utilized to further assess the cellular uptake and trafficking of the BSA633-MP conjugates. As shown in Fig. 6B, we observed onsiderable co-localization of conjugates and Lysotracker, which is a marker for lysosomes. These results indicated that the nanoconjugates were endocytosed and transported through the lysosome pathway.

*Cytoprotective ability of the BSA633-MP conjugates*. We first determined the percentage of apoptosis cells with different doses of PAN during a 48-h period. A dose-dependent decrease in cell viability was observed (Fig. 7A) and 15 $\mu$g/ml of PAN was used in the followed experiments. PAN induced podocyte apoptosis in a time-dependent manner (Fig. 7B). Compared with control cells, there was almost 50% apoptosis after 48 h of exposure to PAN. We next measured the podocyte apoptosis after PAN exposure in the presence of free MP or BSA633-MP conjugate at an equal drug concentration of 1 $\mu$M. As shown in Fig. 7C, MP significantly enhanced cell viability at 48 h by 41.36% (72.69±1.39 vs. 51.42±1.29% without MP, P<0.01). However, the BSA633-MP conjugate showed a relatively weaker cytoprotective ability against PAN-induced apoptosis with an increase in cell viability by 20.07% (61.74±1.13 vs. 51.42±1.29% without BSA633-MP, P<0.01). The toxicity

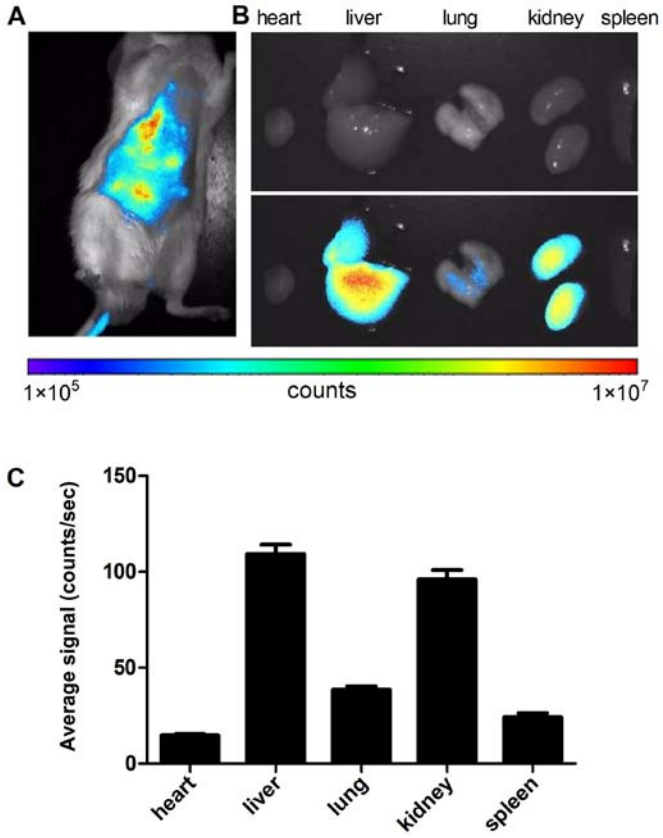


Figure 8. Biodistribution of the BSA633-MP nanoconjugates monitored by fluorescence imaging. (A) *In vivo* imaging, (B) *ex vivo* imaging of excised tissues. From left to right are the heart, liver, lung, kidney and spleen, respectively. The upper row represents a white background. (C) Quantitative analysis of fluorescence imaging values in the different tissues. Data are presented as the mean ± standard error of the mean (n=3)

of the conjugates itself was also examined. There was no significant difference in the viability of cells treated with 1 $\mu$M equivalent MP in conjugates compared with control cells. In addition, the cells treated with the nanoconjugates maintained similar normal morphology as the control cells.

*In vivo biodistribution*. To evaluate whether BSA carrying nanoconjugates can reach the kidney *in vivo*, the infrared dye Alexa Fluor 633-linked BSA nanoconjugate was administered intravenously to normal mice and its *in vivo* biodistribution was estimated by fluorescence imaging. Once 24 h had passed after intravenous injection of BSA633-MP, NIR fluorescence imaging of the intact mice was acquired (Fig. 8A). As expected, the nanoconjugate exhibited strong liver and kidney targeting and relative weaker signals in other organs with low background. The *ex vivo* fluorescence of the dissected organs further confirmed the preferential accumulation of BSA633-MP nanoconjugates in the liver and kidney (Fig. 8B and C). These results indicated that BSA633-MP nanoconjugates possess kidney-targeting ability, which is favorable for improving targeted kidney administration efficacy *in vivo*.

## Discussion

To overcome the severe systemic side effects of GCs used in the therapy of nephrotic syndrome, the present study described a small non-cytotoxic monomolecular nanoconjugate. In the present study, albumin, a specific ligand of the FcRn receptor, which is highly expressed in glomeruli of nephrotic syndrome specimens and cultured human podocytes (Fig. 1), was selected as the carrier and targeting moiety. Methylprednisolone (MP) was selected as a therapeutic entity. Both albumin and MP have been verified as having adequate safety profiles in clinical applications, enabling feasibility of this study. BSA is widely used for drug delivery since it is abundant, has low cost, is biocompatible and easy to link with drugs. Several albumin nanoparticles have been reported for drug delivery, such as adsorption of obidoxime onto human serum albumin (HSA) to form nanoparticles (22), silk fibroin-albumin nanoparticles towards tumor cells (23), and albumin-gentamicin microspheres (24). Abraxane®, a nanoparticulate composite of HSA and paclitaxel, has been approved by the US Food and Drug Administration (FDA) for cancer treatment (25). Although the albumin approach is a well-established method for directing drugs to cancer cells, to our knowledge this is the first study for using albumin for directing an anti-inflammatory drug to podocytes. In the present study, high payloads were realized with multiple MP molecules displayed on one single albumin. The loading efficiency was estimated to be approximately 12 MP molecules per molecule of our nanoconjugates (through MALDI-TOF MS in Fig. 3C).

Through SDS-PAGE and TEM (Fig. 3A and B), the resultant nanoparticles showed a uniform and mono-dispersed size distribution with an average diameter of approximately 10 nm, consistent with their hydrodynamic size. Thus, they are large enough to pass through renal glomerlular filtration in the pathological condition of renal syndrome with damaged filtration barrier. We also used HPLC method to discern between associated drug and conjugated drug. As shown in Fig. 3D, the amount of adhered drug was less than 2%, demonstrating that MP was mainly conjugated to BSA instead of being adhered.

Ideally, a drug delivery system should be stable enough in circulation so that it can be delivered to targeted sites successfully. More importantly, to produce pharmacological actions, the drugs must be released from the delivery system in the target cells so that they can play a therapeutic role. We utilized an acid-sensitive amide bond to link GCs to albumin so that in the acidic environment of cellular lysosomes the linkage can be potentially broken and the GCs released in the target cells. The pH-associated stability assays revealed that the targeted nanoconjugates are stable in neutral pH while the majority of MPs can be released from the nanoconjugates at pH 4.0 (Fig. 4). During endocytosis, the pH change can be exploited through acid cleavage of the amide linker so as to let the drug be released inside the target cells (26).

Uptake assays confirmed the receptor-mediated transportation of the nanoconjugates. The nanoconjugates demonstrated a dose-dependent uptake and a 36-fold enhancement in human podocytes compared to FcRn-negative VSMCs (Fig. 5B). In addition, excess free BSA markedly inhibited uptake of the nanoconjugates (Fig. 5C). These observations support the notion that uptake of the BSA-based nanoconjugates depends on the FcRn receptor-mediated endocytosis. The high FcRn expression in human podocytes suggests that the receptor is an ideal target candidate for directing GC drugs to podocytes.

Furthermore, the use of FcRn for GC entry is supported by the abundant expression of FcRn by our immune fluorescence assay in biopsy specimen (Fig. 2A). It was observed in Fig. 6B that the nanoconjugates were transported to endosomes. Considering that the fluorescent dye Alexa Fluor 633 was linked to albumin instead of the drug, we still could not discern whether the drugs are released from the albumin carrier. Thus, additional studies are needed to reveal the precise trafficking pathways of the nanoconjugates.

PAN is characterized by podocyte apoptosis (9,12). In this study, PAN was used to induce apoptosis in the cultured human podocytes. It has been widely reported that GCs could prevent podocytes from being injured by PAN. Our *in vitro* study showed a positive effect of BSA633-MP on protection of PAN-induced apoptosis. However, the free MP drug proved to be more efficient than the nanoconjugate (Fig. 7C). This may be due to the fact that when entering cells, large molecules require recognition by specific receptors and internalization into the cells, while small free drugs are accessible to the cells through free diffusion. Additionally, it is theoretically impossible for the nanoconjugates to release the linked drugs entirely.

We made an initial investigation of *in vivo* distribution of the nanoconjugates using fluorescence imaging system. Non-invasive molecular imaging is widely recognized as a tool for disease detection in most organs especially cancers (27-32). Biological tissues have lower absorbance and autofluorescence in the near-infrared region (NIR). NIR dyes, small organic molecules that function in the NIR, therefore have received increasing attention in the field of tumor imaging and therapy (33). Our tracer Alexa Fluor 633 demonstrated a high signal-to-background ratio. Results (Fig. 8) showed that the nanoconjugates remained in the kidney 24 h after intravenous injection. According to our design, when glomerluli barriers were damaged, the nanoconjugates passed the renal filtration and entered podocytes through receptor-mediated endocytosis. It must be mentioned that just like discussions in the intracellular trafficking, the biodistribution of nanoconjugates only reflected the situation of the BSA carrier. Yet, the aim of the present study was to provide a preliminary evaluation on the passive targeting of the conjugate. We plan to use HPLC to trace drug distribution in the future when all the prerequisites are ready.

In conclusion, albumin-mediated drug-targeting to the FcRn receptor is a new potential approach for the safe therapy of podocyte-associated kidney diseases. This approach involves development of a low-dose GC therapy with a specific high-dose effect on podocytes, thereby enhancing the beneficial GC effects and reducing severe adverse effects. Although far from clinical application, FcRn expressed by podocytes may potentially offer a therapeutic opportunity.

## Acknowledgements

This study was supported by grants from the National Natural Science Foundation of China (no. 81170660), the Clinical Science and Technology Projects of Jiangsu Province (nos. BL2012032 and BL2014080) and the Priority Academic Program Development (PAPD) of Jiangsu Higher Education Institutions.

## References

1. Hogan J and Radhakrishnan J: The treatment of idiopathic focal segmental glomerulosclerosis in adults. Adv Chronic Kidney Dis 21: 434-441, 2014.
2. Andolino TP and Reid Adam J: Nephrotic syndrome. Pediatr Rev 36: 117-125, 2015.
3. Tran TH, J Hughes G, Greenfeld C and Pham JT: Overview of current and alternative therapies for idiopathic membranous nephropathy. Pharmacotherapy 35: 396-411, 2015.
4. Rezende GM, Viana VS, Malheiros DM, Borba EF, Silva NA, Silva C, Leon EP, Noronha IL and Bonfa E: Podocyte injury in pure membranous and proliferative lupus nephritis: Distinct underlying mechanisms of proteinuria? Lupus 23: 255-262, 2014.
5. Akchurin O and Reidy KJ: Genetic causes of proteinuria and nephrotic syndrome: Impact on podocyte pathobiology. Pediatr Nephrol 30: 221-233, 2015.
6. Yan K, Kudo A, Hirano H, Watanabe T, Tasaka T, Kataoka S, Nakajima N, Nishibori Y, Shibata T, Kohsaka T, *et al*: Subcellular localization of glucocorticoid receptor protein in the human kidney glomerulus. Kidney Int 56: 65-73, 1999.
7. Xing CY, Saleem MA, Coward RJ, Ni L, Witherden IR and Mathieson PW: Direct effects of dexamethasone on human podocytes. Kidney Int 70: 1038-1045, 2006.
8. Ransom RF, Lam NG, Hallett MA, Atkinson SJ and Smoyer WE: Glucocorticoids protect and enhance recovery of cultured murine podocytes via actin filament stabilization. Kidney Int 68: 2473-2483, 2005.
9. Wada T, Pippin JW, Marshall CB, Griffin SV and Shankland SJ: Dexamethasone prevents podocyte apoptosis induced by puromycin aminonucleoside: Role of p53 and Bcl-2-related family proteins. J Am Soc Nephrol 16: 2615-2625, 2005.
10. Agrawal S, Guess AJ, Benndorf R and Smoyer WE: Comparison of direct action of thiazolidinediones and glucocorticoids on renal podocytes: Protection from injury and molecular effects. Mol Pharmacol 80: 389-399, 2011.
11. Liu H, Gao X, Xu H, Feng C, Kuang X, Li Z and Zha X: α-Actinin-4 is involved in the process by which dexamethasone protects actin cytoskeleton stabilization from adriamycin-induced podocyte injury. Nephrology (Carlton) 17: 669-675, 2012.
12. Yu SY and Qi R: Role of bad in podocyte apoptosis induced by puromycin aminonucleoside. Transplant Proc 45: 569-573, 2013.
13. Ohashi T, Uchida K, Uchida S, Sasaki S and Nitta K: Dexamethasone increases the phosphorylation of nephrin in cultured podocytes. Clin Exp Nephrol 15: 688-693, 2011.
14. Mao Y, Triantafillou G, Hertlein E, Towns W, Stefanovski M, Mo X, Jarjoura D, Phelps M, Marcucci G, Lee LJ, *et al*: Milatuzumab-conjugated liposomes as targeted dexamethasone carriers for therapeutic delivery in CD74 B-cell malignancies. Clinical cancer research: Clin Cancer Res 19: 347-356, 2013.
15. Graversen JH, Svendsen P, Dagnæs-Hansen F, Dal J, Anton G, Etzerodt A, Petersen MD, Christensen PA, Møller HJ and Moestrup SK: Targeting the hemoglobin scavenger receptor CD163 in macrophages highly increases the anti-inflammatory potency of dexamethasone. Mol Ther 20: 1550-1558, 2012.
16. Asgeirsdóttir SA, Kamps JA, Bakker HI, Zwiers PJ, Heeringa P, van der Weide K, van Goor H, Petersen AH, Morselt H, Moorlag HE, *et al*: Site-specific inhibition of glomerulonephritis progression by targeted delivery of dexamethasone to glomerular endothelium. Mol Pharmacol 72: 121-131, 2007.
17. Asgeirsdóttir SA, Zwiers PJ, Morselt HW, Moorlag HE, Bakker HI, Heeringa P, Kok JW, Kallenberg CG, Molema G and Kamps JA: Inhibition of proinflammatory genes in anti-GBM glomerulonephritis by targeted dexamethasone-loaded AbEsel liposomes. Am J Physiol Renal Physiol 294: F554-F561, 2008.
18. Wang Y, Tian Z, Thirumalai D and Zhang X: Neonatal Fc receptor (FcRn): A novel target for therapeutic antibodies and antibody engineering. J Drug Target 22: 269-278, 2014.
19. Eyre J, Ioannou K, Grubb BD, Saleem MA, Mathieson PW, Brunskill NJ, Christensen EI and Topham PS: Statin-sensitive endocytosis of albumin by glomerular podocytes. Am J Physiol Renal Physiol 292: F674-F681, 2007.
20. Haymann JP, Levraud JP, Bouet S, Kappes V, Hagège J, Nguyen G, Xu Y, Rondeau E and Sraer JD: Characterization and localization of the neonatal Fc receptor in adult human kidney. J Am Soc Nephrol 11: 632-639, 2000.
21. Wu L, Wu J, Zhou Y, Tang X, Du Y and Hu Y: Enhanced antitumor efficacy of cisplatin by tirapazamine-transferrin conjugate. Int J Pharm 431: 190-196, 2012.

22. Kufleitner J, Wagner S, Worek F, von Briesen H and Kreuter J: Adsorption of obidoxime onto human serum albumin nanoparticles: Drug loading, particle size and drug release. J Microencapsul 27: 506-513, 2010.
23. Subia B and Kundu SC: Drug loading and release on tumor cells using silk fibroin-albumin nanoparticles as carriers. Nanotechnology 24: 035103, 2013.
24. Della Porta G, Adami R, Del Gaudio P, Prota L, Aquino R and Reverchon E: Albumin-gentamicin microspheres produced by supercritical assisted atomization: Optimization of size, drug loading and release. J Pharm Sci 99: 4720-4729, 2010.
25. Kratz F: A clinical update of using albumin as a drug vehicle - a commentary. J Control Release 190: 331-336, 2014.
26. Rodrigues PC, Roth T, Fiebig HH, Unger C, Mülhaupt R and Kratz F: Correlation of the acid-sensitivity of polyethylene glycol daunorubicin conjugates with their *in vitro* antiproliferative activity. Bioorg Med Chem 14: 4110-4117, 2006.
27. Li Y, Du Y, Liu X, Zhang Q, Jing L, Liang X, Chi C, Dai Z and Tian J: Monitoring tumor targeting and treatment effects of IRDye 800CW and GX1-conjugated polylactic acid nanoparticles encapsulating endostar on glioma by optical molecular imaging. Mol Imaging 14: 356-365, 2015.
28. Francisco AF, Lewis MD, Jayawardhana S, Taylor MC, Chatelain E and Kelly JM: Limited ability of posaconazole To cure both acute and chronic *Trypanosoma cruzi* infections revealed by highly sensitive *in vivo* imaging. Antimicrob Agents Chemother 59: 4653-4661, 2015.
29. Zhang C, Liu T, Su Y, Luo S, Zhu Y, Tan X, Fan S, Zhang L, Zhou Y, Cheng T, *et al*: A near-infrared fluorescent heptamethine indocyanine dye with preferential tumor accumulation for *in vivo* imaging. Biomaterials 31: 6612-6617, 2010.
30. Neurath MF: Molecular Endoscopy and *in vivo* Imaging in inflammatory bowel diseases. Dig Dis 33 (Suppl 1): 32-36, 2015.
31. Piwnica-Worms D: From the guest editor: Illuminating cancer in vivo with molecular imaging. Cancer J 21: 150-151, 2015.
32. Chan MM, Gray BD, Pak KY and Fong D: Non-invasive *in vivo* imaging of arthritis in a collagen-induced murine model with phosphatidylserine-binding near-infrared (NIR) dye. Arthritis Res Ther 17: 50, 2015.
33. Yuan A, Wu J, Tang X, Zhao L, Xu F and Hu Y: Application of near-infrared dyes for tumor imaging, photothermal, and photodynamic therapies. J Pharm Sci 102: 6-28, 2013.